ACS Partner Journal
PRECISION CHEMISTRY
Editors' Choice
Open Access

pubs.acs.org/PrecisionChem
Article

Mechanically Stable and Damage Resistant Freestanding Ultrathin Silver Nanowire Films with Closely Packed Crossed-Lamellar Structure

Si-Chao Zhang,[#] Huai-Ling Gao,[#] Long Zhang, Yin-Bo Zhu, Ya-Dong Wu, Jian-Wei Liu, Li-Bo Mao, Mei Feng, Liang Dong, Zhao Pan, Xiang-Sen Meng, Yang Lu,* and Shu-Hong Yu*

Cite This: *Precis. Chem.* 2024, 2, 634−643
Read Online
ACCESS | Metrics & More | Article Recommendations | Supporting Information

ABSTRACT: One-dimensional (1D) functional nanowires are widely used as nanoscale building blocks for assembling advanced nanodevices due to their unique functionalities. However, previous research has mainly focused on nanowire functionality, while neglecting the structural stability and damage resistance of nanowire assemblies, which are critical for the long-term operation of nanodevices. Biomaterials achieve excellent mechanical stability and damage resistance through sophisticated structural design. Here, we successfully prepared a mechanically stabilized monolamella silver nanowire (Ag NW) film, based on a facile bubble-mediated assembly and nondestructive transfer strategy with the assistance of a porous mixed cellulose ester substrate, inspired by the hierarchical structure of biomaterial. Owing to the closely packed arrangement of Ag NWs combined with their weak interfaces, the monolamellar Ag NW film can be transferred to arbitrary substrates without damage. Furthermore, freestanding multilamellar Ag NW films with impressive damage resistance can be obtained from the monolamellar Ag NW film, through the introduction of bioinspired closely packed crossed-lamellar (CPCL) structure. This CPCL structure maximizes intra- and interlamellar interactions among Ag NWs ensuring efficient stress transfer and uniform electron transport, resulting in excellent mechanical durability and stable electrical properties of the multilamellar Ag NW films.

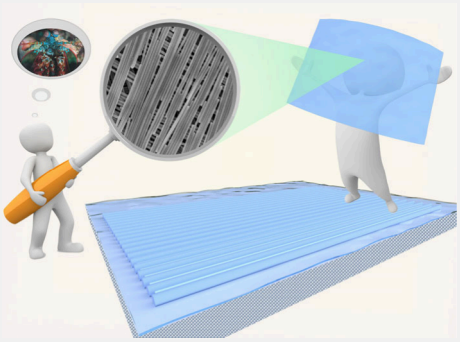

KEYWORDS: *Biomimetics, hierarchical structure, structural stability, damage resistance, functional nanowire assemblies*

INTRODUCTION

With the development of nanotechnology, a series of nanounits with fascinating properties have been synthesized. In order to maximize their unique functions in practical applications, advanced assembly strategies have been developed to assemble them into various nanodevices, bridging the gap from the nano- to the macro-world.[1−4] Among various nanounits, one-dimensional (1D) functional nanowires have attracted much attention due to their large surface-to-volume ratio, unique two-dimensional (2D) confinement, as well as excellent mechanical and electrical properties.[5] It has been verified that oriented assembly of 1D nanowires not only exploits their structural characteristics (i.e., large aspect ratios and anisotropies) for the propagating pathways of quantum particles (photons, electrons and phonons), but also produces new macroscopic properties (electrical, thermal, and optical properties, among others).[6−8]

Considerable efforts have been devoted to the assembly of different 1D functional nanowires into the macroscopic assemblies, demonstrating excellent application potential in various fields.[9−12] For example, A uniformly and periodically assembled tellurium nanowire array exhibited a controllable inverse photoconductive response at amplified optical intensities from the UV to the VIS-IR region, which was considered to be an unusual but interesting phenomenon different from the positive photoconductive effect of conventional semiconductors.[13] By using a unique monomicelle-directed assembly method, the well-ordered corrugated titanium dioxide nanowire arrays were controllably synthesized, which induced a large band bending and efficient surface hole extraction, thus accelerating photocatalytic water splitting reaction kinetics.[14] Orientationally aligned ceramic nanowires prepared by electrostatic spinning technology exhibit excellent ionic conductivity in the lithium-ion batteries.[15] Although significant progress has been made in the functional application of nanowire assemblies,[4,16,17] their structural stability and damage resistance are still understudied.

Received: July 2, 2024
Revised: September 14, 2024
Accepted: September 18, 2024
Published: October 13, 2024

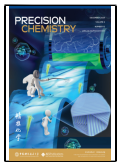

https://doi.org/10.1021/prechem.4c00053
Precis. Chem. 2024, 2, 634−643

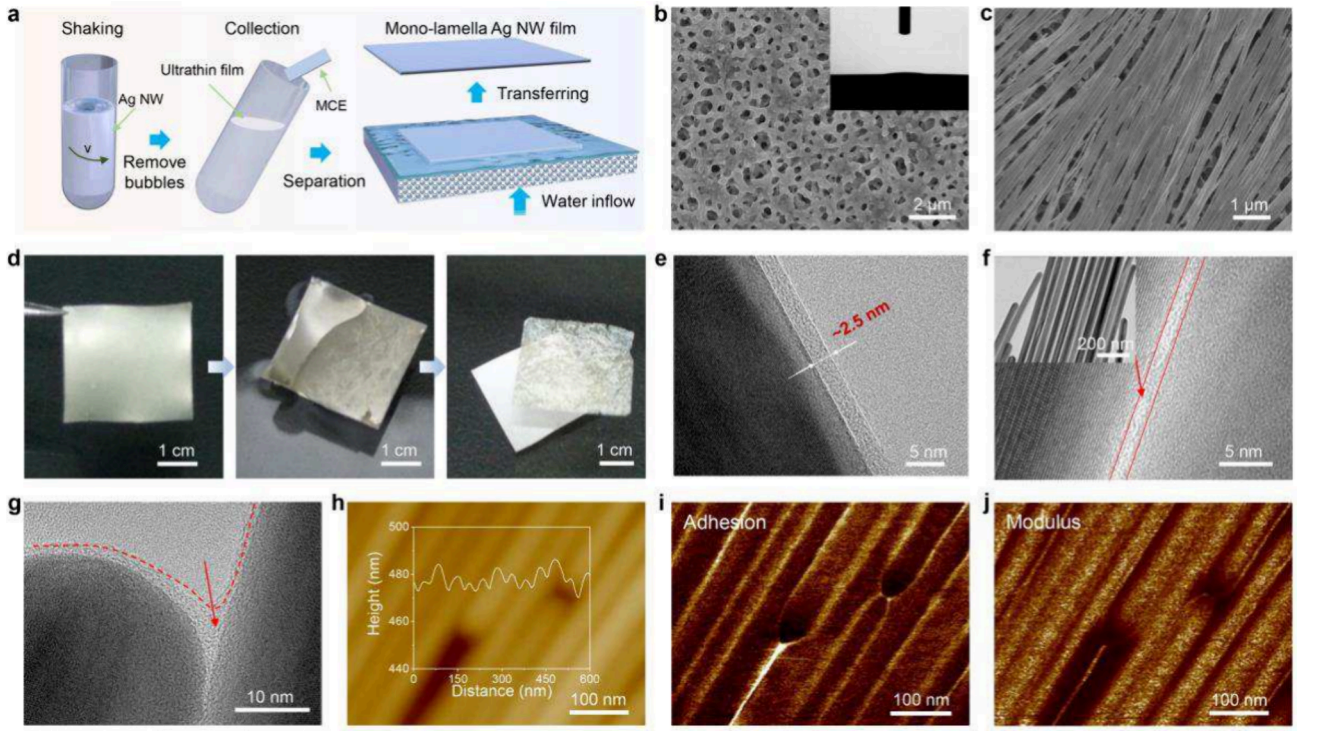

Figure 1. Fabrication and characterization of monolamellar Ag NW film. (a) Schematic representation of bubble-mediated assembly and nondestructive transfer method. (b) SEM image of the surface of commercial MCE, showing uniform nanopores structure. The inset image indicates the water contact angle of the MCE membrane. (c) Assembled monolamellar Ag NW film on porous MCE substrate. (d) Monolamellar Ag NW film was separated from the porous MCE substrate in water. (e–g) HRTEM images of single Ag NW (e) and monolamellar Ag NW film (f,g). The arrows indicate the PVP layer. (h–j) High sensor (h), adhesion (i), and modulus (j) of monolamellar Ag NW film. Diagram shows the height sensor is smaller than Ag NW diameter, and the high adhesion and low modulus of adjacent Ag NW edge indicate the interaction between two adjacent Ag NWs.

Biological structural materials achieve excellent damage resistance[18] and structural stability[19−21] through various strategies such as elemental gradient distribution,[22] weak interfaces,[23] and densely packed nanounits with high orderliness.[24] Herein, we introduced biomimetic hierarchical structures into the assembly of silver nanowires (Ag NWs), aiming to estimate the positive effects of the biomimetic design on the mechanical stability and damage resistance of macroscopic functional nanowire assemblies. We first obtain a transferable monolamella Ag NW film with closely packed structures based on a facile, green bubble-mediated assembly and nondestructive transfer method assisted by a highly hydrophilic and easily separable porous mixed cellulose ester (MCE) substrate. Densely packed Ag NWs and polyvinylpyrrolidone (PVP)-mediated weak interfaces stabilize the monolamellar structure, guaranteeing nondestructive transfer. For a wide range of application scenes, the closely packed cross-lamellar (CPCL) structural design of the biological structure principle is introduced to obtain structurally stable and damage resistant multilamellar Ag NW film. This biomimetic structure provides a large number of intra- and interlamellar interactions among Ag NWs by maximizing their contact areas, achieving efficient stress transfer and uniform electron transport. The multilamellar Ag NW films exhibit excellent mechanical durability and stable electrical properties even under 10,000 bending fatigue cycles.

RESULTS AND DISCUSSION

First of all, we present a facile, green bubble-mediated assembly and nondestructive transfer strategy for the construction of monolamellar film (Figure 1a). Ag NWs (55 nm in diameter and 4 μm in length) were used as a typical 1D NW to validate the effectiveness of this strategy (Figure S1). In contrast to the previous Langmuir–Blodgett (LB) assembly that involved volatile organic reagents and high loss of raw materials (partial nanounits were wasted due to their own gravitational sinking),[25,26] we utilized only vibration-generated bubbles to accomplish the Ag NWs interfacial assembly without using any reagents. The unassembled Ag NWs were kept in suspension for the next bubble-mediated assembly without any waste. Specifically, the Ag NW suspension (4 mg mL^{-1}) was shaken in an oscillator (250 times/min) to produce abundant bubbles. The presence of bubbles significantly extended the surface area of the gas–liquid interface to facilitate NW assembly.[27] Ag NWs can float stably at the gas–liquid interface due to surface tension. When bubbles were removed by centrifugation or resting (Figure 1a and Figure S2), the Ag NWs resting on the bubble surface were released to the solution surface and subsequently merged to form a continuous and compact Ag NW layer with bright metallic luster.

In order to collect the floated Ag NW lamella and subsequently nondestructive transfer, the substrate should be selected with superior hydrophilicity and separable characteristics. Porous MCE membrane was thoughtfully selected as the substrate due to its good water permeability and porous surface

https://doi.org/10.1021/prechem.4c00053
Precis. Chem. 2024, 2, 634−643

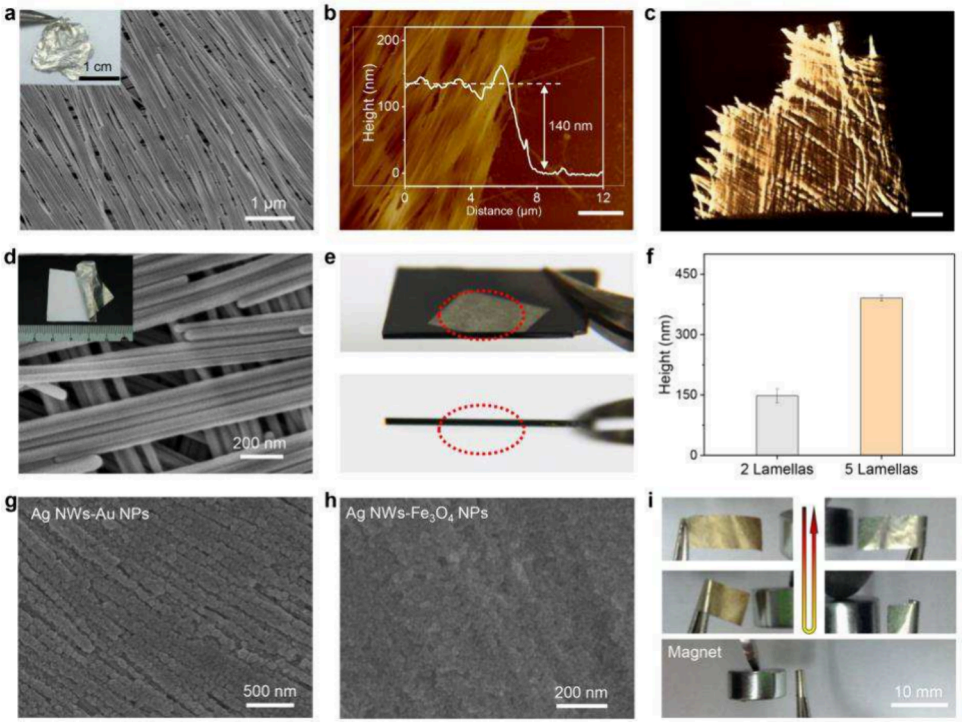

Figure 2. Fabrication and characterization of biomimetic Ag NW films. (a) SEM image of 2-lamellar Ag NW film, inset shows the freestanding properties of the film. (b) AFM image of a 2-lamellar Ag NW film and the inset diagram represents the film thickness of the white rectangular box area. The scale bar was 2 μm. (c) Soft X-ray microscopy (Nano-CT) image shows the edge of a 2-lamellar Ag NW film. The scale bar was 2 μm. (d) SEM image of 5-lamellar Ag NW film. The inset image indicates easily obtainable 5-lamellar Ag NW film from MCE membrane. (e) 5-lamellar Ag NW film transferred onto a silicon wafer. (f) The average thickness of 2-lamellar and 5-lamellar Ag NW films derived from height mapping of AFM images. (g,h) Ag NW films as versatile substrate for coassembly of Au (g) and Fe_3O_4 (h) nanoparticles. (i) Flexible response of 5-lamellar Ag NW film loaded with Fe_3O_4 nanoparticles to external magnetic fields.

(Figure 1b). The resulting Ag NW lamella with bright metallic luster was confirmed to have a highly ordered and uniform arrangement of only monolamellar Ag NW, and Ag NWs in the monolamella were closely compacted with each other along their longitudinal direction (Figure 1c). After drying, the porous characteristics of the MCE membrane allowed the collected Ag NW lamella to be easily separated from the MCE substrate by simple water impregnation (Figure 1d). Benefiting from the interactions between ligands on the surface of the Ag NWs, the monolamellar Ag NW film can remain integral in water without disintegrating and can be easily transferred to different substrates without any pretreatment (Figure S3a–c). Dense MCE membrane, obtained by dissolution regeneration, collected monolamellar Ag NW film did not separate at the air–water interface and sank directly to the bottom of water (Figure S3d–f). Analogous to dense MCE membranes, monolamellar Ag NW films collected from other types of substrates were also difficult to separate at the interface (Figure S4). As a result, this porous MCE substrate not only maintains superior hydrophilicity for the collection of monolamellar Ag NW film but also weakens interaction between the substrate and monolamellar Ag NW film by reducing contact area, which guarantees the subsequent nondestructive transfer without any pretreatment.

To explore the intrinsic mechanism of this method, we have conducted a detailed study of the monolamellar Ag NW film interaction. As depicted in Figure 1e, a high-resolution transmission electron microscopy (HRTEM) image indicates the surface of the Ag NW contains a PVP layer, which was derived from the synthesis process of Ag NWs. This thin layer of PVP molecules was considered to maintain the structural stability of the Ag NW through the interaction between oxygen and silver atoms.[28] Compared to single Ag NW, thinner PVP layers were present among the Ag NWs of monolamellar Ag NW film (Figure 1f,g and Figure S5), indicating PVP molecules are supposed to entangle with each other to form a dense PVP network.[29] Therefore, the presence of the PVP layer not only stabilizes a single nanowire but also serves as a bridge connecting different NWs. According to the atomic force microscope (AFM) quantitative nanomechanical mapping test, the Ag NW edges showed significantly higher adhesion to AFM tip due to the presence of PVP layer (Figure S6). Compared with the smooth height mapping (Figure 1h), a large difference at the edges of Ag NWs in the adhesion mapping was still maintained in the monolamellar Ag NW film (Figure 1i). Modulus mapping of monolamellar Ag NW film shows lower modulus for the PVP layer compared to Ag NW (Figure 1j), which is similar to the weak interfaces of highly inorganic minerals in teeth[22] and bone.[30] The presence of weak interfaces increases the path of crack propagation, which increases the damage resistance of the material.[31] The weak interface between neighboring Ag NWs, originated from the thin PVP layer, ensures the structural stability of the monolamellar Ag NW film without brittle rupture even under stirring (Movie S1).

Considering that various scenarios require different forms of functional nanowire assemblies, freestanding films are widely used as an economical and efficient form of assemblies in numerous fields.[32−34] The closely packed biomineralized nanowires in each lamella of the bovine enamel and land

https://doi.org/10.1021/prechem.4c00053
Precis. Chem. 2024, 2, 634−643

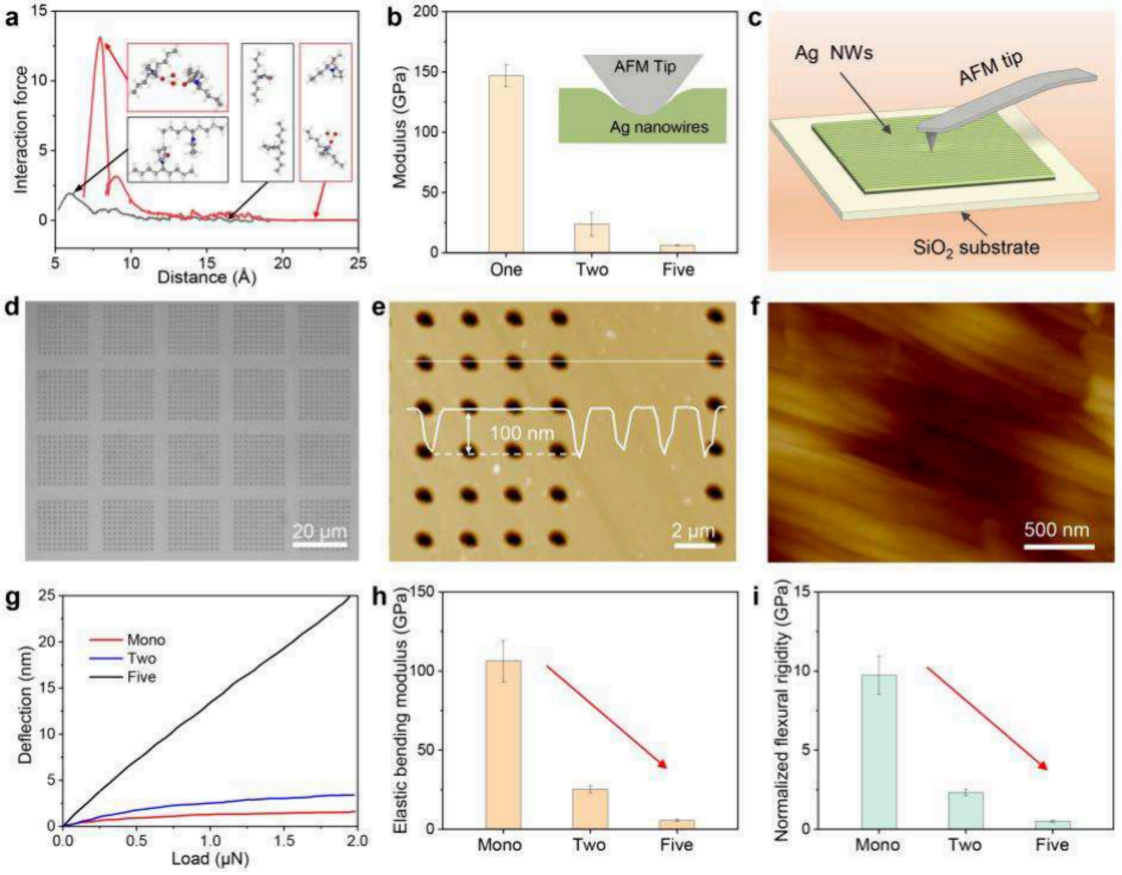

Figure 3. Mechanical stability of the biomimetic Ag NW films. (a) Simulation of interaction forces between two PVP molecules during a uniaxial tension with (red line) and without (black line) hydrogen bond (kcal/(mol·Å)). (b) AFM modulus of different lamellar Ag NW films. (c) Schematic representation of the AFM bending test for different lamellar Ag NW films. (d,e) Optical microscope (d) and AFM (e) images of different Si/SiO_2 substrates (1 μm in diamater, 100 nm in depth) originating from lithography. (f) AFM image of monolamellar Ag NW film on the Si/SiO_2 substrate (Z-scale: 200 nm). (g) Displacement-load curves of different lamellar Ag NW films from the AFM force curve. The curve was smoothed through three points. (h,i) Elastic bending modulus (h) and normalized flexural rigidity (i) of different lamellar Ag NW films.

snail (*Bradybaena similaris*) shells impart the organism superior structural stability and damage resistance[35] through the CPCL structure (Figure S7). Consequently, we considered introducing this interlamellar structural design principle underlying monolamellar Ag NW film to increase the interaction among adjacent lamellas and thus prepared damage-resistant freestanding Ag NW films for complex scenes. These Ag NW films with CPCL structure can be prepared by sequential multiple collection of Ag NW lamellas from the gas−liquid interface (Figure S8). Interestingly, a freestanding Ag NW film with a simple CPCL microstructure was obtained from the MCE substrate by careful exfoliation after drying (Figure 2a). The thickness of the freestanding Ag NW film was measured to be only ∼140 nm (Figure 2b), which meant only two lamellas of Ag NWs. Soft X-ray nanotomography reveals that the interlamellar cross-packing and intralamellar parallel arrangement of Ag NWs directly cover a large area (Figure 2c), and macroscopic Ag NW film presents an isotropic structure (Figure S9). This is similar to the definition of quasicrystals for short-range ordered and long-range unordered.[36]

The Ag NW film exhibited a stable freestanding property when collecting five lamellas (Figure 2d), which was invisible to the naked eye from the cross section after being transferred onto a silicon wafer (Figure 2e). The thickness of this freestanding Ag NW film was measured to be ∼390 nm (Figure 2f). Scanning electron microscope (SEM) images from top and cross section views clearly reveal the highly ordered arrangement of Ag NWs in the short-range and a uniform structure in the long-range (Figures S10 and S11). According to quantitative measurement of a series of Ag NW films (Figure S12), the close linear correlation between the silver mass per unit area and the lamellar number confirmed the fact that this Ag NW film is composed of only five Ag NW lamellas. The similar volume density of the 5-lamellar Ag NW film (∼8.38 g cm^{-3}) relative to that of bulk silver (Table S1) provided further evidence for the closely packed arrangement of Ag NWs. As the reference, disordered Ag NW film was made by vacuum filtration using the same Ag NW suspension and substrate until it can be peeled off.[37] Due to the thin thickness and close packing of Ag NWs, the silver mass per unit area of 5-lamellar Ag NW film (∼3.27 μg mm^{-2}) is much lower than disordered Ag NW film (∼19.05 μg mm^{-2}, Table S1), which is a solid demonstration of the economical fabricating processes. In addition, these freestanding Ag NW films can also be employed as versatile substrates for coassembly of a series of functional nanoparticles to fabricate multifunctional films, which not only possess new functionalities but also retain their inherent unique performances (Figure 2g−i).

To clearly investigate the relationship between the CPCL microstructure and mechanical properties, detailed mechanical tests were used to analyze the structural stability and damage

https://doi.org/10.1021/prechem.4c00053
Precis. Chem. 2024, 2, 634−643

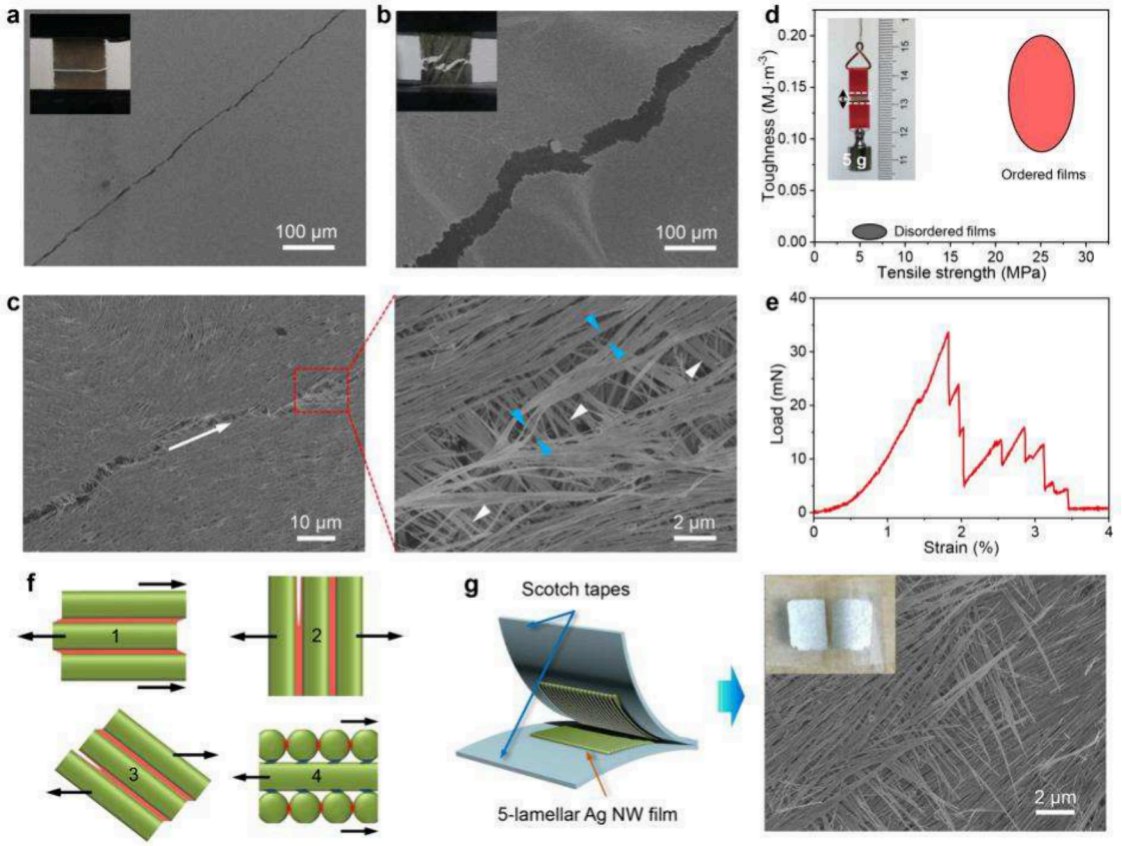

Figure 4. Damage resistance of the biomimetic Ag NW films. (a,b) SEM images with the same resolution show different fracture path in disordered (a) and 5-lamellar (b) Ag NW films in mechanical tearing tests. (c) SEM images show typical debonding and pullout of Ag NWs at the crack tip of 5-lamellar Ag NW film. Red arrow indicates the crack extension direction, blue arrows indicate the debonding of Ag NWs, white arrows indicate the pullout of Ag NWs. (d) Ashby diagram of toughness versus tensile strength for disorderd and 5-lamellar Ag NW films. Insert digital image shows a small piece of 5-lamellar Ag NW film (6 mm in width and only 400 nm in thickness) hangs up a 5 g weight. (e) Typical sawtooth pattern on the load−displacement curve in mechanical tearing tests. (f) Schematic illustrations show the occurrences of intralaminar frictional sliding and debonding, respectively (1, 2) or synergistically (3), and interlamina frictional sliding in multilamellar Ag NW film (4) which are resistant to tearing. (g) The 5-lamellar Ag NW film is separated into two slices by mechanical exfoliation, and the ladder-shaped exfoliated surface is widely observed by SEM image.

resistance mechanisms of biomimetic Ag NW films. Molecular dynamics simulations indicated that there are van der Waals forces and stronger hydrogen bond interactions between two adjacent PVP molecules (Figure 3a), which closely resembles the strengthening and toughening mechanism of silk based on dense hydrogen bonding networks.[38] This synergistic effect of van der Waals forces and hydrogen bonds would lead to unique interfacial interactions in the CPCL structure. The interfacial interactions generated between adjacent Ag NWs in Ag NW films with CPCL structures can be divided into two types, intralamellar interaction between parallel-attached Ag NWs in each lamella and interlamellar interactions between crossed-attached Ag NWs in two adjacent lamellas (Figure S13). Compared to fewer interfacial interactions in disordered Ag NW film due to random stacking of Ag NWs (Figure S14), this well-designed CPCL structure would maximize the intralamellar and the interlamellar interactions through contacting as many areas as possible, facilitating efficient stress transfer between adjacent Ag NWs. Therefore, the Ag NW film with a CPCL structure maintains structural integrity even at extreme conditions (Figure S15).

To quantitatively visualize the structural stability of Ag NW films, AFM modulus was used to evaluate the intralamellar and interlamellar interactions. As shown in Figure 3b, the modulus decreases gradually as the number of stacked lamellas increases. AFM bending tests were used to test the bending behavior of Ag NW films under the applied biaxial stress (Figure 3c), which are important to verify structural integrity.[39,40] The Si/SiO_2 substrates with periodic circular holes were prepared by lithography (Figure 3d,e). For obtaining smooth samples on the Si/SiO_2 substrate, the water-mediated nondestructive transfer method was used for the transfer of different lamellar Ag NW films. The Ag NW film above the hole was imaged to pinpoint the center of the circle (maximum displacement) while maintaining the tip-to-sample force of 2 μN. The structure integrity of the monolamellar Ag NW film was destroyed under biaxial stress when the pore diameter of the Si/SiO_2 substrate was 5 μm (Figure S16). This is unfavorable to study intralamellar stress transfer of the CPCL structure, and the Si/SiO_2 substrate with a diameter of 1 μm and a depth of 100 nm was chosen (Figure 3f). According to the displacement-force curves, the bending deflection degree of the Ag NW film increases with the lamella number (Figure 3g), indicating that the Ag NW film gradually softens with the increase in the number of lamellas. The bending modulus and flexural rigidity of the Ag NW film were used to quantify the extent of this softening. It was found that the performance of the Ag NW film showed a gradual decrease with the increase of

https://doi.org/10.1021/prechem.4c00053
Precis. Chem. 2024, 2, 634−643

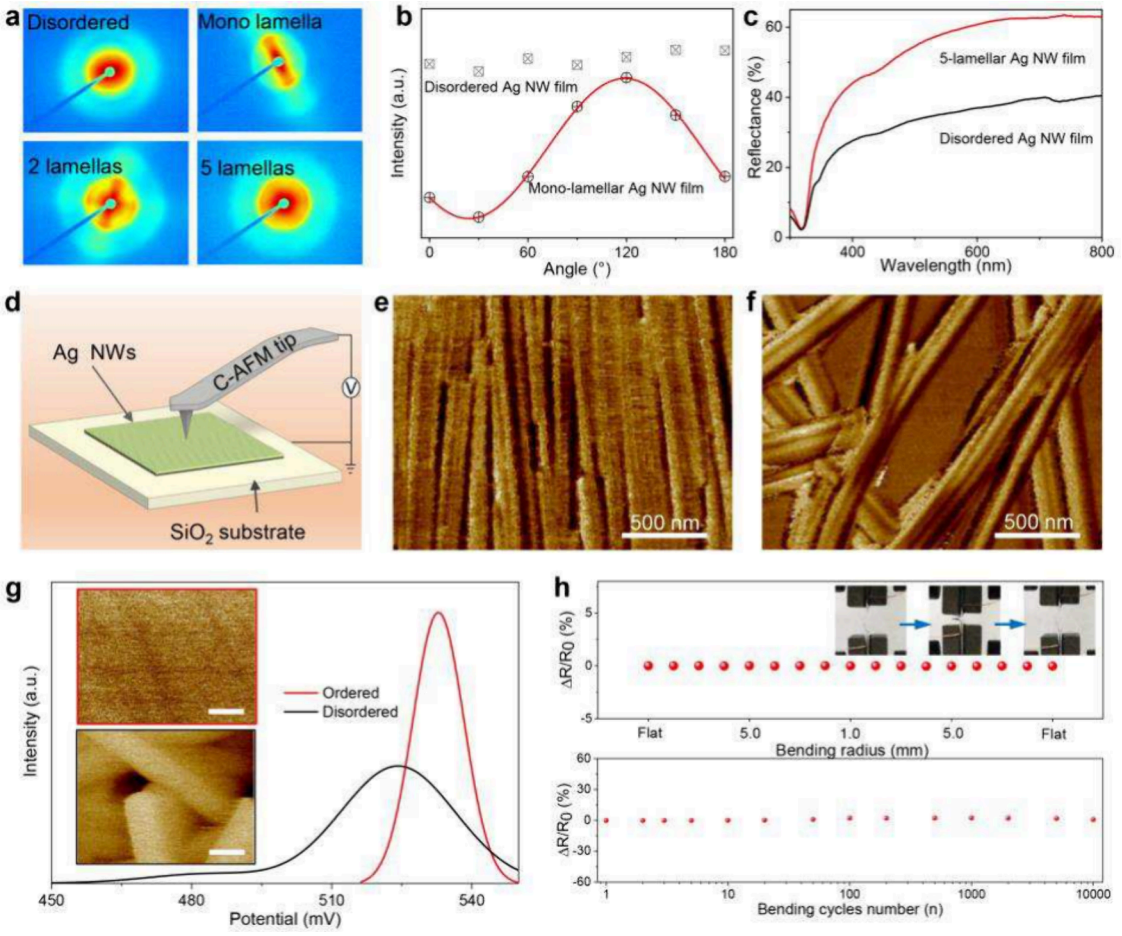

Figure 5. Functional superiority of the biomimetic Ag NW films. (a) 2D SAXS patterns of different Ag NW film. (b) Optical polarization curves at transmission mode of monolamellar Ag NW film (black square spots) and disordered Ag NW film (black box spots). The monolamellar Ag NW film is similar to a polarizer, and the transmission intensity peaks when the polarization direction rotated in parallel with the arranged direction of Ag NWs in the monolamella. (c) Reflectance spectra of 5-lamellar and disordered Ag NW film. (d) Schematic representation of the conducting AFM (C-AFM) for different lamellar Ag NW film. (e,f) Current mappings of monolamellar (e) and disordered (f) Ag NW film were constructed by a Pt−Ir-coated tip at the sample bias of +1 V. (g) Distribution of potential for monolamellar (red line) and disordered (black) Ag NW films. The inseted diagrams represent the potential images of monolamellar (red box) and disordered (black box) Ag NW film. The scale bar was 100 nm. (h) Mechanical flexibility and stability of the 5-lamellar Ag NW film. Electrical resistance as a function of the bending cycles at a maximum bending radius of 1.0 mm. Inset shows photographs of the bending process of the 5-lamellar Ag NW film.

lamella number. The elastic bending modulus and normalized flexural rigidity of the Ag NW films displayed an exponential decrease from monolamella to 2-lamellas (Figure 3h,i).

Different from the strong interactions generated by the closely packed Ag NWs within the intralamellas, the interlamellar interactions generated by the confined contact areas of the Ag NWs dampen the stress transfer (Figure S13). From the perspective of view of stress transfer, the contact areas between neighboring Ag NWs should be increased and the lamella number of Ag NW films should be decreased, maximizing the transfer and dissipation of stress. It is predictable that disordered Ag NW films with fewer contact areas have worse stress transfer, which leads to poorer mechanical properties. Therefore, 5-lamellar Ag NW film has achieved stable structure and freestanding properties with as few lamellas as possible, through NW closely packed interlamella and intralamella.

To explore the damage resistance of the CPCL structure, 5-lamellar Ag NW films and disordered Ag NW films were used for fracture and tear analysis. In contrast to an approximate straight fracture path in the disordered Ag NW film (Figure 4a), a highly tortuous fracture surface in the 5-lamellar Ag NW film was observed (Figure 4b). This tortuosity, namely crack deflection, was identified as a dominant toughening mechanism in natural biomaterials.[31,41] It is anticipated that the deflection of the crack path partly distributed the applied force with a long distance of load transmission due to the high aspect ratio of the 1D NWs, which would be effective in promoting retardation and crack arrest. In situ SEM observation further demonstrated the sawtooth fracture path of a 5-lamellar Ag NW film during the tearing process in contrast to that of a disordered Ag NW film (Movie S2). Crack tip at higher magnification reveals the typical debonding and pullout of the individual Ag NWs in each lamella (Figure 4c and Figure S17). Static tensile tests were further performed to quantitatively investigate the enhancement of mechanical strength from the molecular scale to the macroscale. For the 5-lamellar Ag NW films, the ultimate tensile strength reaches up to 24.8 ± 3.8 MPa, and toughness reaches to 0.145 ± 0.055 MJ m^{-3}, which is much higher than that of disordered Ag NW films (Figure 4d).

Furthermore, the crack deflection was detected by recording the change of loading force in the process of mechanical

https://doi.org/10.1021/prechem.4c00053
Precis. Chem. 2024, 2, 634−643

tearing, and a typical sawtooth pattern in load−displacement curve[31,42] was obtained (Figure 4e). The lowering of stress was identified as the sequential fracture of the Ag NW interfaces. As schematically illustrated in Figure 4f, frictional sliding and debonding between adjacent Ag NWs in each lamella happened during the interfacial destruction, while interlamellar frictional sliding occurred between two adjacent Ag NW lamellas. With the synergistic effect of intralamellar and interlamellar frictional sliding, cracks tend to propagate preferentially along the weaker Ag NW boundaries, and then lead to crack deflection.[43] After mechanical exfoliation with tape, the tearing surface of the 5-lamellar Ag NW film showed a trapezoidal peeled surface to increase the difficulty of peeling (Figure 4g). These mechanisms are associated with the CPCL structure of the Ag NW films, which guided the crack growth and arrest, and efficiently increased damage resistance.[44]

Synchrotron-based small-angle X-ray scattering (SAXS) was used to analyze their short-range structure ordering information.[45] Compared to the isotropic microstructure of disordered Ag NW films, different lamellar Ag NW films exhibited an obvious anisotropic microstructure (Figure 5a and Figure S18). The transmission intensity of the monolamellar Ag NW film showed typically periodic variation of sine wave at different polarization angles (Figure 5b). For the 2-lamellar Ag NW film, the deflection angle between adjacent lamella was ∼85°, which reflected the spatial cross arrangement of Ag NWs in the top lamella and the bottom lamella (Figure S18b). These structural features were expected to provide optical activity, and were ideal candidates for chiral sensor design.[46] The reflectivity of the 5-lamellar Ag NW film was significantly increased compared with the disordered Ag NW film (Figure 5c), which was expected to provide excellent high-reflectivity conductive coatings for nonconductive surfaces in photovoltaic field.[47]

To understand the electrical superiority of the Ag NW films with CPCL structure, conductive AFM (C-AFM) was used to examine the spatial distribution of the Ag NW film currents (Figure 5d). Samples for the C-AFM measurements were disordered/mono-/2-lameller Ag NW films, and current mapping was constructed by a Pt−Ir-coated tip at the sample bias of +1 V. For monolamellar and 2-lamellar Ag NW films, the preferential current flow was observed through the Ag NWs with a relatively uniform contribution to the current (Figure 5e and Figure S19). In contrast, the disordered Ag NW film sample had a nonuniform current distribution (Figure 5f), and many dead areas (current offered by the Si substrate) were visible. Dead regions in mono- and 2-lamellar samples were much fewer in number relative to those in the disordered sample, which implies that the uniformly aligned Ag NWs in mono- and 2-lamellar samples provide continuous paths for electron transport, lowering the charge transfer resistance, thus promising to improve the conductivity and kinetics of the electrodes.[12] Meanwhile, the Ag NW films with ordered structures exhibited homogeneous potential distribution compared to the disordered Ag NW film (Figure 5g), which was considered to be more prone to generate uniform built-in electric field beneficial for the charge separation and transportation.[48]

The fatigue resistance of the 5-lamellar freestanding films was then evaluated by measuring the film resistance under various working conditions. The resistance values of the 5-lamellar Ag NW films (freestanding or attached to an elastic membrane) were maintained constant even when exposed to a high-volume environment of 110 dB (Figure S20). Furthermore, there was no obvious change of the resistance at a bending radius of 1.0 mm after 10,000 bending cycles (Figure 5h and Movie S3), indicating stable mechanical and electrical properties under cyclic bending stress. Combined mechanical and electrical superiority, the freestanding ultrathin Ag NW films are regarded to have significant potential as current collectors in lithium−metal batteries (Figure S21).

CONCLUSION

In summary, we assembled Ag NWs, a typical kind of functional 1D NWs, into a macroscopic ultrathin Ag NW film with hierarchical structure by proposing a facile, green bubble-mediated assembly and nondestructive transfer strategy with the assistance of a porous MCE substrate. Benefiting from the closely packed NWs and the weak interface mediated by the PVP molecules, the monolamellar Ag NW film exhibited a stable structure, facilitating its easy transfer to arbitrary substrates. Multilamellar freestanding Ag NW films were obtained through introducing a biological CPCL structure with high damage resistance in a monolamellar film. These freestanding Ag NW films with CPCL structure could form a large number of intralamellar and interlamellar interactions among Ag NWs, leading to great mechanical stability and damage resistance. The structural stability of these freestanding Ag NW films provides an important guarantee of their functional properties. As a validation, we demonstrated the stable long-term application performance of the multilamellar Ag NWs as current collector for lithium batteries.

ASSOCIATED CONTENT

Supporting Information

The Supporting Information is available free of charge at https://pubs.acs.org/doi/10.1021/prechem.4c00053.

Experimental methods, SEM image of the Ag NW, nature model, fabrication process of Ag NW film, microstructure of multilamellar and disordered Ag NW film, interactions and intermolecular reinforcement mechanism of Ag NW film, AFM bending test of Ag NW film, crack extension and structure characterization of Ag NW film, current mappings of disordered and multilamellar Ag NW structure, stability of 5-lamellar Ag NW film, electrochemistry Performance of Cu−Li and Ag−Li electrode (PDF)

Video showing mono-lamellar Ag NW film without brittle rupture under stirring (MP4)

Video showing the destruction of the disordered Ag NW film and the freestanding 5-lamellar Ag NW film (MP4)

Video showing the mechanical flexibility and stability of the freestanding 5-lamellar Ag NW film (MP4)

AUTHOR INFORMATION

Corresponding Authors

Yang Lu − *Anhui Key Laboratory of Controllable Chemical Reaction and Material Chemical Engineering, School of Chemistry and Chemical Engineering, Hefei University of Technology, Hefei, Anhui 230009, P. R. China;* orcid.org/0000-0002-8412-809X; Email: yanglu@hfut.edu.cn

Shu-Hong Yu − *Department of Chemistry, New Cornerstone Science Laboratory, Institute of Biomimetic Materials & Chemistry, Anhui Engineering Laboratory of Biomimetic*

https://doi.org/10.1021/prechem.4c00053
Precis. Chem. 2024, 2, 634−643

Materials, Division of Nanomaterials & Chemistry, Hefei National Research Center for Physical Sciences at the Microscale, University of Science and Technology of China, Hefei 230026, China; Institute of Innovative Materials (I2M), Department of Chemistry, Department of Materials Science and Engineering, Southern University of Science and Technology, Shenzhen 518055, China; orcid.org/0000-0003-3732-1011; Email: shyu@ustc.edu.cn

Authors

Si-Chao Zhang − *Department of Chemistry, New Cornerstone Science Laboratory, Institute of Biomimetic Materials & Chemistry, Anhui Engineering Laboratory of Biomimetic Materials, Division of Nanomaterials & Chemistry, Hefei National Research Center for Physical Sciences at the Microscale, University of Science and Technology of China, Hefei 230026, China*

Huai-Ling Gao − *Department of Chemistry, New Cornerstone Science Laboratory, Institute of Biomimetic Materials & Chemistry, Anhui Engineering Laboratory of Biomimetic Materials, Division of Nanomaterials & Chemistry, Hefei National Research Center for Physical Sciences at the Microscale, University of Science and Technology of China, Hefei 230026, China; CAS Key Laboratory of Mechanical Behavior and Design of Materials, Department of Modern Mechanics, CAS Center for Excellence in Complex System Mechanics, University of Science and Technology of China, Hefei 230027, China;* orcid.org/0000-0001-8908-1967

Long Zhang − *Department of Chemistry, New Cornerstone Science Laboratory, Institute of Biomimetic Materials & Chemistry, Anhui Engineering Laboratory of Biomimetic Materials, Division of Nanomaterials & Chemistry, Hefei National Research Center for Physical Sciences at the Microscale, University of Science and Technology of China, Hefei 230026, China*

Yin-Bo Zhu − *CAS Key Laboratory of Mechanical Behavior and Design of Materials, Department of Modern Mechanics, CAS Center for Excellence in Complex System Mechanics, University of Science and Technology of China, Hefei 230027, China;* orcid.org/0000-0001-9204-9300

Ya-Dong Wu − *Anhui Key Laboratory of Controllable Chemical Reaction and Material Chemical Engineering, School of Chemistry and Chemical Engineering, Hefei University of Technology, Hefei, Anhui 230009, P. R. China*

Jian-Wei Liu − *Department of Chemistry, New Cornerstone Science Laboratory, Institute of Biomimetic Materials & Chemistry, Anhui Engineering Laboratory of Biomimetic Materials, Division of Nanomaterials & Chemistry, Hefei National Research Center for Physical Sciences at the Microscale, University of Science and Technology of China, Hefei 230026, China;* orcid.org/0000-0001-9237-1025

Li-Bo Mao − *Department of Chemistry, New Cornerstone Science Laboratory, Institute of Biomimetic Materials & Chemistry, Anhui Engineering Laboratory of Biomimetic Materials, Division of Nanomaterials & Chemistry, Hefei National Research Center for Physical Sciences at the Microscale, University of Science and Technology of China, Hefei 230026, China;* orcid.org/0000-0002-9249-2449

Mei Feng − *Department of Chemistry, New Cornerstone Science Laboratory, Institute of Biomimetic Materials & Chemistry, Anhui Engineering Laboratory of Biomimetic Materials, Division of Nanomaterials & Chemistry, Hefei National Research Center for Physical Sciences at the Microscale, University of Science and Technology of China, Hefei 230026, China*

Liang Dong − *Department of Chemistry, New Cornerstone Science Laboratory, Institute of Biomimetic Materials & Chemistry, Anhui Engineering Laboratory of Biomimetic Materials, Division of Nanomaterials & Chemistry, Hefei National Research Center for Physical Sciences at the Microscale, University of Science and Technology of China, Hefei 230026, China*

Zhao Pan − *Department of Chemistry, New Cornerstone Science Laboratory, Institute of Biomimetic Materials & Chemistry, Anhui Engineering Laboratory of Biomimetic Materials, Division of Nanomaterials & Chemistry, Hefei National Research Center for Physical Sciences at the Microscale, University of Science and Technology of China, Hefei 230026, China*

Xiang-Sen Meng − *Department of Chemistry, New Cornerstone Science Laboratory, Institute of Biomimetic Materials & Chemistry, Anhui Engineering Laboratory of Biomimetic Materials, Division of Nanomaterials & Chemistry, Hefei National Research Center for Physical Sciences at the Microscale, University of Science and Technology of China, Hefei 230026, China*

Complete contact information is available at: https://pubs.acs.org/10.1021/prechem.4c00053

Author Contributions

[#]S.-C.Z. and H.-L.G. contributed equally to this work. S.-H.Y., Y.L., S.-C.Z., and H.-L.G. conceived the idea and designed the experiments, S.-H.Y. supervised the research, S.-C.Z., H.-L.G. and Y.L. carried out the synthesis and characterizations of samples, S.-C.Z. and H.-L.G. performed the mechanical testing and electronic measurement, L.Z. help to perform the electrochemical analysis. Y.B.Z. performed the simulation, Y.-D.W., M.F., L.D. and Z.P. help to prepare the samples, J.-W.L., L.-B.M. and X.-S.M. helped to perform the structural analysis, S.-C.Z., H.-L.G., Y.L., and S.-H.Y. analyzed data and cowrote the paper. All authors discussed the results.

Funding

This work was supported by the National Key Research and Development Program of China (2021YFA0715700), the Strategic Priority Research Program of the Chinese Academy of Sciences (Grants XDB0450402), the National Natural Science Foundation of China (22293044, 21975241, 22222508), the Fundamental Research Funds for the Central Universities (WK2340000112), the Major Basic Research Project of Anhui Province (2023z04020009), the New Cornerstone Investigator Program.

Notes

The authors declare no competing financial interest.

■ ACKNOWLEDGMENTS

This work was partially carried out at the USTC Center for Micro and Nanoscale Research and Fabrication. The authors would like to thank Gang Chen (ShanghaiTech University), Zhen He (Southern University of Science and Technology) for SAXS analysis, Yong Guan (National Synchrotron Radiation Laboratory of USTC) for Nano CT analysis, Wei-Hong Xu and Wei Shen (Hefei Institute of Intelligent Machines, Chinese Academy of Sciences) for in situ SEM observation, Tao Ma (Chaohu University) for electrochemical analysis.

■ ABBREVIATIONS

1D, one-dimensional; 2D, two-dimensional; Ag NW, silver nanowire; CPCL, closely packed crossed-lamellar; MCE, mixed cellulose ester; SEM, Scanning electron microscope; HRTEM, high-resolution transmission electron microscopy; PVP, polyvinylpyrrolidone; AFM, atomic force microscope; C-AFM, conductive AFM; SAXS, small-angle X-ray Scattering.

■ REFERENCES

(1) Cheng, X.; Fan, Z.; Yao, S.; Jin, T.; Lv, Z.; Lan, Y.; et al. Programming 3D curved mesosurfaces using microlattice designs. *Science* **2023**, *379* (6638), 1225−1232.

(2) Nepal, D.; Kang, S.; Adstedt, K. M.; Kanhaiya, K.; Bockstaller, M. R.; Brinson, L. C.; et al. Hierarchically structured bioinspired nanocomposites. *Nat. Mater.* **2023**, *22* (1), 18−35.

(3) Wang, W.; Jiang, Y.; Zhong, D.; Zhang, Z.; Choudhury, S.; Lai, J.-C.; et al. Neuromorphic sensorimotor loop embodied by monolithically integrated, low-voltage, soft e-skin. *Science* **2023**, *380* (6646), 735−742.

(4) Jia, C.; Lin, Z.; Huang, Y.; Duan, X. Nanowire Electronics: From Nanoscale to Macroscale. *Chem. Rev.* **2019**, *119* (15), 9074−9135.

(5) Wang, J.-L.; Hassan, M.; Liu, J.-W.; Yu, S.-H. Nanowire Assemblies for Flexible Electronic Devices: Recent Advances and Perspectives. *Adv. Mater.* **2018**, *30* (48), 1803430.

(6) He, Z.; Yang, Y.; Liang, H.-W.; Liu, J.-W.; Yu, S.-H. Nanowire Genome: A Magic Toolbox for 1D Nanostructures. *Adv. Mater.* **2019**, *31* (51), 1902807.

(7) Glotzer, S. C.; Solomon, M. J. Anisotropy of building blocks and their assembly into complex structures. *Nat. Mater.* **2007**, *6* (8), 557−562.

(8) Liu, Z.; Xu, J.; Chen, D.; Shen, G. Flexible electronics based on inorganic nanowires. *Chem. Soc. Rev.* **2015**, *44* (1), 161−192.

(9) Liu, J.-W.; Liang, H.-W.; Yu, S.-H. Macroscopic-Scale Assembled Nanowire Thin Films and Their Functionalities. *Chem. Rev.* **2012**, *112* (8), 4770−4799.

(10) Tian, B.; Lieber, C. M. Nanowired Bioelectric Interfaces. *Chem. Rev.* **2019**, *119* (15), 9136−9152.

(11) Quan, L. N.; Kang, J.; Ning, C.-Z.; Yang, P. Nanowires for Photonics. *Chem. Rev.* **2019**, *119* (15), 9153−9169.

(12) Zhou, G.; Xu, L.; Hu, G.; Mai, L.; Cui, Y. Nanowires for Electrochemical Energy Storage. *Chem. Rev.* **2019**, *119* (20), 11042−11109.

(13) Wang, R.; Wang, J.-L.; Liu, T.; He, Z.; Wang, H.; Liu, J.-W.; et al. Controllable Inverse Photoconductance in Semiconducting Nanowire Films. *Adv. Mater.* **2022**, *34* (36), 2204698.

(14) Zhang, P.; Tian, Z.; Kang, Y.; He, B.; Zhao, Z.; Hung, C.-T.; et al. Sub-10 nm Corrugated TiO2 Nanowire Arrays by Monomicelle-Directed Assembly for Efficient Hole Extraction. *J. Am. Chem. Soc.* **2022**, *144* (45), 20964−20974.

(15) Liu, W.; Lee, S. W.; Lin, D.; Shi, F.; Wang, S.; Sendek, A. D.; et al. Enhancing ionic conductivity in composite polymer electrolytes with well-aligned ceramic nanowires. *Nat. Energy* **2017**, *2* (5), 17035.

(16) He, Z.; Wang, J.-L.; Chen, S.-M.; Liu, J.-W.; Yu, S.-H. Self-Assembly of Nanowires: From Dynamic Monitoring to Precision Control. *Acc. Chem. Res.* **2022**, *55* (11), 1480−1491.

(17) Shin, J.; Kang, N.; Kim, B.; Hong, H.; Yu, L.; Kim, J.; et al. One-dimensional nanomaterials for cancer therapy and diagnosis. *Chem. Soc. Rev.* **2023**, *52* (13), 4488−4514.

(18) Fratzl, P.; Kolednik, O.; Fischer, F. D.; Dean, M. N. The mechanics of tessellations − bioinspired strategies for fracture resistance. *Chem. Soc. Rev.* **2016**, *45* (2), 252−267.

(19) Shi, N. N.; Tsai, C.-C.; Camino, F.; Bernard, G. D.; Yu, N.; Wehner, R. Keeping cool: Enhanced optical reflection and radiative heat dissipation in Saharan silver ants. *Science* **2015**, *349* (6245), 298−301.

(20) Eder, M.; Amini, S.; Fratzl, P. Biological composites-complex structures for functional diversity. *Science* **2018**, *362* (6414), 543−547.

(21) Meng, X.-S.; Zhou, L.-C.; Liu, L.; Zhu, Y.-B.; Meng, Y.-F.; Zheng, D.-C.; et al. Deformable hard tissue with high fatigue resistance in the hinge of bivalve Cristaria plicata. *Science* **2023**, *380* (6651), 1252−1257.

(22) DeRocher, K. A.; Smeets, P. J. M.; Goodge, B. H.; Zachman, M. J.; Balachandran, P. V.; Stegbauer, L.; et al. Chemical gradients in human enamel crystallites. *Nature* **2020**, *583* (7814), 66−71.

(23) Barthelat, F.; Yin, Z.; Buehler, M. J. Structure and mechanics of interfaces in biological materials. *Nat. Rev. Mater.* **2016**, *1* (4), 16007.

(24) Ling, S.; Kaplan, D. L.; Buehler, M. J. Nanofibrils in nature and materials engineering. *Nat. Rev. Mater.* **2018**, *3* (4), 18016.

(25) Oliveira, O. N., Jr.; Caseli, L.; Ariga, K. The Past and the Future of Langmuir and Langmuir−Blodgett Films. *Chem. Rev.* **2022**, *122* (6), 6459−6513.

(26) Yang, J.; Chang, L.; Zhang, X.; Cao, Z.; Jiang, L. Ionic Liquid-Enhanced Assembly of Nanomaterials for Highly Stable Flexible Transparent Electrodes. *Nano-Micro Lett.* **2024**, *16* (1), 140.

(27) Zhu, E.; Liu, Y.; Huang, J.; Zhang, A.; Peng, B.; Liu, Z.; et al. Bubble-Mediated Large-Scale Hierarchical Assembly of Ultrathin Pt Nanowire Network Monolayer at Gas/Liquid Interfaces. *ACS Nano* **2023**, *17* (14), 14152−14160.

(28) Huang, H. H.; Ni, X. P.; Loy, G. L.; Chew, C. H.; Tan, K. L.; Loh, F. C.; et al. Photochemical formation of silver nanoparticles in poly(N-vinylpyrrolidone). *Langmuir* **1996**, *12* (4), 909−912.

(29) Zhang, Z.; Fu, Y.; Yu, W.; Qin, X.; Xue, Z.; Liu, Y.; et al. Dynamically Regulated Ag Nanowire Arrays for Detecting Molecular Information of Substrate-Induced Stretched Cell Growth. *Adv. Mater.* **2016**, *28* (43), 9589−9595.

(30) Wang, R.; Gupta, H. S. Deformation and Fracture Mechanisms of Bone and Nacre. *Annu. Rev. Mater. Res.* **2011**, *41*, 41−73.

(31) Wegst, U. G.; Bai, H.; Saiz, E.; Tomsia, A. P.; Ritchie, R. O. Bioinspired structural materials. *Nat. Mater.* **2015**, *14* (1), 23−36.

(32) Yang, Z.; Zhao, C.; Qu, Y.; Zhou, H.; Zhou, F.; Wang, J.; et al. Trifunctional Self-Supporting Cobalt-Embedded Carbon Nanotube Films for ORR, OER, and HER Triggered by Solid Diffusion from Bulk Metal. *Adv. Mater.* **2019**, *31* (12), 1808043.

(33) Park, K.-S.; Kang, J.-G.; Choi, Y.-J.; Lee, S.; Kim, D.-W.; Park, J.-G. Long-term, high-rate lithium storage capabilities of TiO2 nanostructured electrodes using 3D self-supported indium tin oxide conducting nanowire arrays. *Energy Environ. Sci.* **2011**, *4* (5), 1796−1801.

(34) Jia, H.; Yang, X.; Kong, Q.-Q.; Xie, L.-J.; Guo, Q.-G.; Song, G.; et al. Free-standing, anti-corrosion, super flexible graphene oxide/silver nanowire thin films for ultra-wideband electromagnetic interference shielding. *J. Mater. Chem. A* **2021**, *9* (2), 1180−1191.

(35) Ren, J.; Wang, Y.; Yao, Y.; Wang, Y.; Fei, X.; Qi, P.; et al. Biological Material Interfaces as Inspiration for Mechanical and Optical Material Designs. *Chem. Rev.* **2019**, *119* (24), 12279−12336.

(36) Bindi, L.; Steinhardt, P. J.; Yao, N.; Lu, P. J. Natural Quasicrystals. *Science* **2009**, *324* (5932), 1306−1309.

(37) De, S.; Higgins, T. M.; Lyons, P. E.; Doherty, E. M.; Nirmalraj, P. N.; Blau, W. J.; et al. Silver Nanowire Networks as Flexible, Transparent, Conducting Films: Extremely High DC to Optical Conductivity Ratios. *ACS Nano* **2009**, *3* (7), 1767−1774.

(38) Keten, S.; Xu, Z. P.; Ihle, B.; Buehler, M. J. Nanoconfinement controls stiffness, strength and mechanical toughness of beta-sheet crystals in silk. *Nat. Mater.* **2010**, *9* (4), 359−367.

(39) Jiang, C.; Markutsya, S.; Pikus, Y.; Tsukruk, V. V. Freely suspended nanocomposite membranes as highly sensitive sensors. *Nat. Mater.* **2004**, *3* (10), 721−728.

(40) Lee, C.; Wei, X.; Kysar, J. W.; Hone, J. Measurement of the Elastic Properties and Intrinsic Strength of Monolayer Graphene. *Science* **2008**, *321* (5887), 385−388.

(41) Koester, K. J.; Ager, J. W.; Ritchie, R. O. The true toughness of human cortical bone measured with realistically short cracks. *Nat. Mater.* **2008**, *7* (8), 672−677.

(42) Mirkhalaf, M.; Dastjerdi, A. K.; Barthelat, F. Overcoming the brittleness of glass through bio-inspiration and micro-architecture. *Nat. Commun.* **2014**, *5*, 3166.

https://doi.org/10.1021/prechem.4c00053
Precis. Chem. 2024, 2, 634−643

(43) Nalla, R. K.; Kruzic, J. J.; Kinney, J. H.; Ritchie, R. O. Mechanistic aspects of fracture and R-curve behavior in human cortical bone. *Biomaterials* **2005**, *26* (2), 217−31.
(44) Arola, D.; Bajaj, D.; Ivancik, J.; Majd, H.; Zhang, D. Fatigue of biomaterials: Hard tissues. *Int. J. Fatigue* **2010**, *32* (9), 1400−1412.
(45) Li, T.; Senesi, A. J.; Lee, B. Small Angle X-ray Scattering for Nanoparticle Research. *Chem. Rev.* **2016**, *116* (18), 11128−80.
(46) Lv, J.; Hou, K.; Ding, D.; Wang, D.; Han, B.; Gao, X.; et al. Gold Nanowire Chiral Ultrathin Films with Ultrastrong and Broadband Optical Activity. *Angew. Chem., Int. Ed.* **2017**, *56* (18), 5055−5060.
(47) İkizler, B.; Erden, S. Simple and additive-free synthesis of highly reflective thin silver films and their application on large-scale surfaces. *Mater. Today Chem.* **2024**, *35*, 101859.
(48) Zhang, Z.; Chen, X.; Zhang, H.; Liu, W.; Zhu, W.; Zhu, Y. A Highly Crystalline Perylene Imide Polymer with the Robust Built-In Electric Field for Efficient Photocatalytic Water Oxidation. *Adv. Mater.* **2020**, *32* (32), 1907746.

https://doi.org/10.1021/prechem.4c00053
Precis. Chem. 2024, 2, 634−643